PHOTONICS Research

Plasmonic anapole states of active metamolecules

Gui-Ming Pan,[1,†] Fang-Zhou Shu,[1,†] Le Wang,[1] Liping Shi,[2,4] and Andrey B. Evlyukhin[3,5]

[1]College of Optical and Electronic Technology, China Jiliang University, Hangzhou 310018, China
[2]Key Laboratory of 3D Micro/Nano Fabrication and Characterization of Zhejiang Province, School of Engineering, Westlake University, Hangzhou 310024, China
[3]Institute of Quantum Optics, Liebniz University Hannover, 30167 Hannover, Germany
[4]e-mail: shiliping@westlake.edu.cn
[5]e-mail: a.b.evlyukhin@daad-alumni.de

Received 10 December 2020; revised 8 March 2021; accepted 8 March 2021; posted 8 March 2021 (Doc. ID 416256); published 29 April 2021

Anapole states, accompanied by strong suppression of light scattering, have attracted extensive attention in recent years due to their supreme performance in enhancing both linear and nonlinear optical effects. Although both low- and high-order anapole states are observed in the dielectric particles with high refractive index, so far few studies have touched on the topic of plasmonic anapole states. Here we demonstrate theoretically and numerically that the ideal plasmonic anapole states (strong suppression of electric dipole scattering) can be achieved in metallic metamolecules via increasing the coupling strength between Cartesian electric dipole and toroidal dipole moments of the system. The increasing coupling is based on compensation of ohmic losses in a plasmon system by introducing of a gain material, the influence of which is well described by the extended coupled oscillator model. Due to suppression of dipole radiation losses, the excitation of anapole states in plasmonic systems can result in enhancement of the near fields in subwavelength spatial regions outside of nanoparticles. That is especially important for developments of nonlinear nanophotonic and plasmonic devices and active functional metamaterials, which provide facilities for strong light energy concentration at the nanoscale. Development of the considered anapole effect with increase of metamolecule components is discussed.

https://doi.org/10.1364/PRJ.416256

1. INTRODUCTION

The control of light propagation and concentration due to surface-plasmon resonances has great implication for the fundamentals and applications of nanophotonics [1,2]. In this context, Mie resonances from the optical spectral range [3–6], supported by high-index dielectric nanoparticles and nanostructures, also attract significant attention from the research community [7]. There are light scattering similarities between plasmonic (metallic) particles and their dielectric counterparts. In the both cases the light scattering can be considered as a light reradiation by multipole sources excited in a scatterer by external incident waves. In this case the total scattered fields are imagined to be a superposition of the fields generated by every multipole moment of the scatterer. As a result, the total and differential scattering cross sections can be decomposed on separate contributions related to certain multipole moments. Such multipole approaches can significantly simplify the analysis of the light scattering process and provide important information about material, shape, and size parameters of scattering nanoparticles and nanostructures. However, there are several principal differences between optical response of metal and dielectric nanoparticles. If for metal nanoparticles the optical response is determined by excitation of the free electron conductive current absorbing light energy due to ohmic losses, the optical reaction of all-dielectric nanoparticles is associated with excitation of the displacement currents without the losses of absorption. In the last case, the linear light–matter interaction is solely determined by scattering. Importantly, the strong electromagnetic fields are concentrated in the near-field zone around metal nanoparticles at the resonant conditions [8], whereas the enhancement of the fields for all-dielectric nanoparticles at the resonant conditions is realized in their volumes [5]. The different optical reactions of the metal and dielectric nanoparticles result in differences of their functional properties used in practical applications [9,10].

Recently, the anapole states are observed in many high-refractive-index dielectric particles that support both electric and magnetic resonances and have zero damping loss [11–13]. An ideal anapole state is known as a state with complete scattering cancellation in the far-field and nonzero near-field excitation. From the theoretical point of view, the typical properties of anapole states exhibit zero polarized multipole moments and high near-field enhancement inside the region occupied by the

scatterers [11,14–16]. The zero polarized moments of anapole states on any dimensionality could constitute the basis of dark matter in the universe [17]. Based on the nonradiative traits, anapole states are increasingly applied to the fields of nonlinear nanophotonics, dielectric metamaterials, light harvesting, and sensing [15,18–23]. In addition, the total suppressed electric dipole (ED) moment, due to the dipole anapole effect, contributes to the achievement of pure magnetic dipole (MD) scattering [14]. Due to the differences between the optical responses of metallic and dielectric nanoparticles and nanostructures, anapole states have so far been carefully studied, mainly in dielectric nanoparticles with a high refractive index and their structures. In particular, strong ohmic losses of metal nanostructures are the main reason for hindering implementation of the anapole analog in metal nanostructures.

Generally, anapole states, including electric and magnetic anapole states, consist of low- and high-order multipoles [15,24–26]. For example, the excitation of electric and magnetic anapole states in a hybrid metal-dielectric structure is theoretically investigated in our previous work [15]. The key to exciting anapole states relies on the effective generation of toroidal dipole (TD) moments, which can be imagined as high-order dipole terms of the Cartesian multipole decomposition [20,27–32]. In the case of electric anapole states, they are realized due to the totally destructive interference between Cartesian TD and ED moments, resulting in significant suppression of the total ED moment and corresponding dipole scattering [11,29,30]. Importantly, the excitation of the TD moment is accompanied by the circulating magnetic field in scattering systems [33–35]. Therefore, formally the existence of electric anapole states can be expected even in metallic metamolecules that support optical resonances accompanied by the circulating magnetic field in the metamolecule volume [36,37]. Nevertheless, the anapole condition cannot be fully satisfied in the lossy system due to the different sensitivities of different-order multipole moments to ohmic losses.

In this paper, we demonstrate both analytically and numerically that the plasmonic anapole states (suppression of the electric dipole scattering) can be excited in metallic metamolecules consisting of several nanoparticles by enhancing the destructive interference between Cartesian ED and TD moments of the total system. It is worth mentioning that the excitation of anapole states in this work is independent of high-refractive-index dielectric nanoparticles. The ideal plasmonic anapole state is achieved when the coupling strength between Cartesian ED and TD moments reaches its maximum value. Due to the different sensitivities of ohmic losses between Cartesian ED (low-order electric mode) and TD (higher-order electric mode) moments [33], the coupling strength can be enhanced by the reasonable compensation of ohmic losses of the nanosystem (0.008 eV^2 for the passive case and 0.014 eV^2 for the active case). This process is well characterized by the extended coupled oscillator (ECO) model [38]. Compared to the anapole states of high-refractive-index nanoparticle origin, the plasmonic anapole states induce stronger intensity of near fields outside nanoparticles due to the participation of surface plasmons.

2. SUPPRESSION OF ELECTRIC DIPOLE SCATTERING

Schematic diagrams of the Au and Au–SiO_2 heptamer are shown in the insets of Fig. 1. The structural parameters selected in the calculation are compatible with current nanofabrication technology [39]. The heights of Au and SiO_2 nanodisks are $h_1 = 50$ nm and $h_2 = 30$ nm, respectively. The diameter of the central disk is $2R = 208$ nm. It is symmetrically surrounded by six nanodisks with an equal diameter of $2r = 195$ nm. The gap between the central disk and the surrounding ones is set to $g = 20$ nm. A monochromatic plane wave with time dependence in the view of $e^{-i\omega t}$ polarized along the y axis illuminates the sample from the Au side, where ω is the angular frequency. The heptamer is suspended in air with the refractive index of 1. The SiO_2 disks doped with a gain material act as a host medium. The refractive index of the SiO_2 doping with a gain material, such as rare-earth ions Pr^{3+}, Ho^{3+}, Er^{3+}, Eu^{2+}, Nd^{3+}, and Tm^{3+}, is described by $n = 1.43 - i\kappa$, where κ denotes the gain coefficient [40]. The gain material dominates the imaginary part of the effective refractive index [41]. The refractive index data describing the optical response of Au is given by Johnson and Christy [42].

The multipole decomposition of the light scattering cross section is calculated in spherical coordinates with using the finite element method (FEM) performed by the commercial COMSOL Multiphysics software. After numerical calculation of the total electric field $\mathbf{E}(\mathbf{r})$ inside all disks of the structure, the spherical multipoles are obtained by numerical integration of the following expressions [43]:

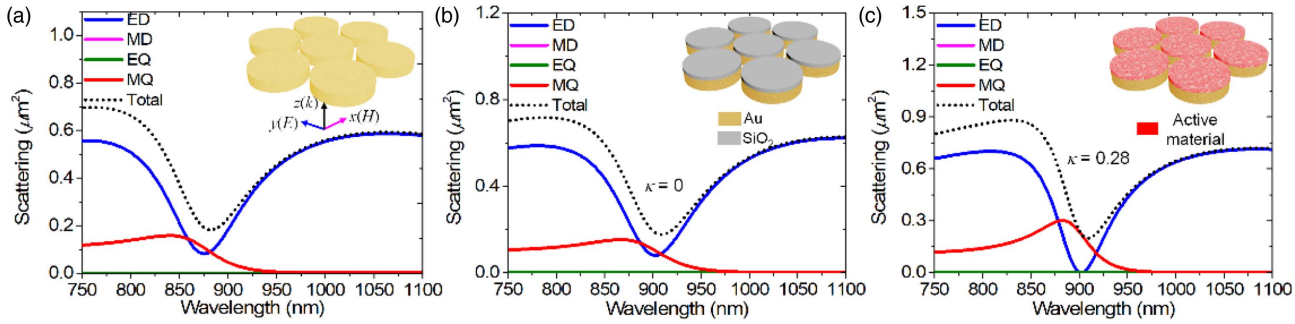

Fig. 1. Scattering cross sections and their spherical multipole decomposition calculated for (a) Au heptamer, (b) passive Au–SiO_2 heptamer with gain coefficient $\kappa = 0$, and (c) active Au–SiO_2 heptamer with gain coefficient $\kappa = 0.28$. The structure schematics are shown in the insets.

$$a(l,m)=\frac{(-i)^{l-1}k^2Z_0O_{lm}}{E_0[\pi(2l+1)]^{1/2}}\times\int e^{-im\varphi}\left\{\left[\psi_l(kr)+\psi_l''(kr)\right]P_l^m(\cos\theta)\hat{r}\cdot\mathbf{J}_{\mathrm{sca}}(\mathbf{r})+\frac{\psi'_l(kr)}{kr}\left[\frac{\mathrm{d}}{\mathrm{d}\theta}P_l^m(\cos\theta)\hat{\theta}\cdot\mathbf{J}_{\mathrm{sca}}(\mathbf{r})-i\frac{m}{\sin\theta}P_l^m(\cos\theta)\hat{\varphi}\cdot\mathbf{J}_{\mathrm{sca}}(\mathbf{r})\right]\right\}\mathrm{d}^3r, \tag{1}$$

$$b(l,m)=\frac{(-i)^{l+1}k^2Z_0O_{lm}}{E_0[\pi(2l+1)]^{1/2}}\int e^{-im\phi}j_l(kr)\left[i\frac{m}{\sin\theta}P_l^m(\cos\theta)\hat{\theta}\cdot\mathbf{J}_{\mathrm{sca}}(\mathbf{r})+\frac{\mathrm{d}}{\mathrm{d}\theta}P_l^m(\cos\theta)\hat{\phi}\cdot\mathbf{J}_{\mathrm{sca}}(\mathbf{r})\right]\mathrm{d}^3r, \tag{2}$$

where l denotes the order of the multipole components, such as dipole ($l=1$) and quadrupole ($l=2$). $\mathbf{J}_{\mathrm{sca}}(\mathbf{r})=-i\omega[\varepsilon(\mathbf{r})-\varepsilon_h]\mathbf{E}(\mathbf{r})$ (ε_h is the dielectric constant of the surrounding medium) and $Z_0=\sqrt{\mu_0/\varepsilon_0\varepsilon_h}$ are the scattering current density and impedance, respectively. O_{lm} reads $O_{lm}=[(2l+1)(l-m)!/(l+m)!]^{1/2}[4\pi l(l+1)]^{-1/2}$. $\psi_l(kr)$ is given by the Riccati–Bessel function. $P_l^m(\cos\theta)$ are the associated Legendre polynomials. E_0 is the electric field amplitude of the incident light. θ and ϕ are the zenith angle and azimuthal angle, respectively. The electric and magnetic multipole scattering cross sections are expressed as $C_E=\frac{\pi}{k^2}\sum_{l=1}^{\infty}\sum_{m=-l}^{l}(2l+1)|a(l,m)|^2$ and $C_M=\frac{\pi}{k^2}\sum_{l=1}^{\infty}\sum_{m=-l}^{l}(2l+1)|b(l,m)|^2$, respectively. We consider that all of the electric and magnetic multipoles are located at the center of mass of the Au–SiO_2 metamolecules.

The scattering cross sections and corresponding spherical multipole expansions are shown in Fig. 1. The total scattering cross section of the Au heptamer exhibits a dip at the wavelength about 850 nm with nonzero spherical ED scattering [see Fig. 1(a)]. To dope the gain material, the low-refractive-index SiO_2 layer is introduced to the Au heptamer [see Figs. 1(b) and 1(c)]. As SiO_2 has weak optical response at the near-infrared wavelengths, the SiO_2 disks in the nanostructure basically play the role of host medium of the gain materials. The introduction of the SiO_2 layer leads to the redshift of the dip. In the passive nanostructure, the total scattering cross section exhibits a dip at the wavelength about 900 nm with nonzero spherical ED scattering [see Fig. 1(b)]. In contrast, when a gain material with the coefficient of 0.28 is introduced to the nanosystem, the ED scattering is completely suppressed at the wavelength of total scattering dip as shown in Fig. 1(c).

3. EXCITATION OF PLASMONIC ANAPOLE

For explanation of the ED scattering suppression we use the multipole decomposition in the framework of the Cartesian multipoles determined in the long wavelength approximation (LWA) [29]. In this case the full Cartesian ED moment can be presented as a sum of infinite series of dipole terms [44,45]. For a relatively small scatterer, the series can be restricted to only the first several terms. If we take only the first two terms, the full electric dipole moment can be approximated by the following expression: $\mathbf{D}=\mathbf{p}+ik\mathbf{T}$ [29]. Then the electric dipole part of the scattering cross section is given by

$$\sigma_{\mathrm{sca}}^{\mathrm{ED}}=\frac{c^2k^4Z_0}{6\pi I_0}|\mathbf{p}+ik\mathbf{T}|^2, \tag{3}$$

where I_0 and c are the illumination intensity and the speed of light in a vacuum, respectively. The Cartesian electric dipole moment $\mathbf{p}$ reads $\mathbf{p}=-\int\mathrm{d}^3r\mathbf{J}_{\mathrm{sca}}(\mathbf{r})/i\omega$, and the electric toroidal dipole moment $\mathbf{T}$ reads $\mathbf{T}=\int\mathrm{d}^3r\{[\mathbf{r}\cdot\mathbf{J}_{\mathrm{sca}}(\mathbf{r})]\mathbf{r}-2r^2\mathbf{J}_{\mathrm{sca}}(\mathbf{r})\}/10c$. When achieving the anapole condition, that is, $\mathbf{p}=-ik\mathbf{T}$, the destructive superposition of the Cartesian electric and toroidal dipoles leads to the cancellation of the full electric dipole moment of the nanosystem and its contribution into the scattering cross section.

The contributions of the spherical ED and the Cartesian (LWA) ED and TD terms in the scattering cross sections of the passive and active nanostructures are shown in Fig. 2. In the passive case [Fig. 2(a)], the anapole state cannot be effectively excited. The total (spherical) ED scattering exists in all considered spectral ranges because the TD contribution does not reach the contribution of the Cartesian ED in the scattering cross section and does not provide the destructive interference. In this case, because of the sensitivity of the TD moment to the ohmic losses, its contribution in the scattering cross section is essentially suppressed and the anapole state is not realized. However, according to Fig. 2(b), there is about π phase difference between $\mathbf{p}$ and $ik\mathbf{T}$ at the wavelength of 900 nm, indicating the destructive interference. The anapole condition may be achieved with the compensation of the ohmic losses in the active structure [Fig. 2(c)]. When the anapole condition is satisfied, the corresponding gain coefficient reaches a so-called "gain threshold." There are two intersections of the Cartesian TD and ED contributions in the scattering cross sections at 900 nm and 925 nm. But only at the 900 nm wavelength is the full (spherical) ED scattering totally suppressed, indicating the anapole realization [it is indicated by a black dash line shown in Fig. 2(c)]. In this case the values of $\mathbf{p}$ and $ik\mathbf{T}$ are equal to each other, but their contributions in the scattereing cross section cancel each other out due to the phase difference π between them [Fig. 2(d)]. It should be noted that the overcompensation of optical losses ($\kappa>0.28$) will lead to the mismatch of the anapole condition, and the ED scattering cannot be totally suppressed. Besides, note that the anapole state stems from the interference between inherent modes of the Au heptamer. According to Fig. 1(a), the anapole states are excited without the assistance of a high-refractive-index dielectric, which is fundamentally different from the previous works [34,35]. As SiO_2 has weak optical response at the near-infrared wavelength, the SiO_2 disks in the nanostructure basically play the role of host medium of the gain materials. To compare the properties of anapole states of metallic metamolecules and high-refractive-index particles, we also calculate the anapole state in a silicon (with the refractive index of 3.5) nanosphere as shown in Fig. 2(e). According to Fig. 2(e), the anapole state can be also fixed at 900 nm when the diameter of the silicon nanosphere is 387 nm. The phase difference between $\mathbf{p}$ and $ik\mathbf{T}$ is π as shown in Fig. 2(f). Since a typical feature of anapole states is energy concentration, the plasmonic anapole states take it to a greater extreme. According to the insets of Fig. 2, the enhancement of the near field induced by the anapole state of metallic metamolecules is much stronger than that inside

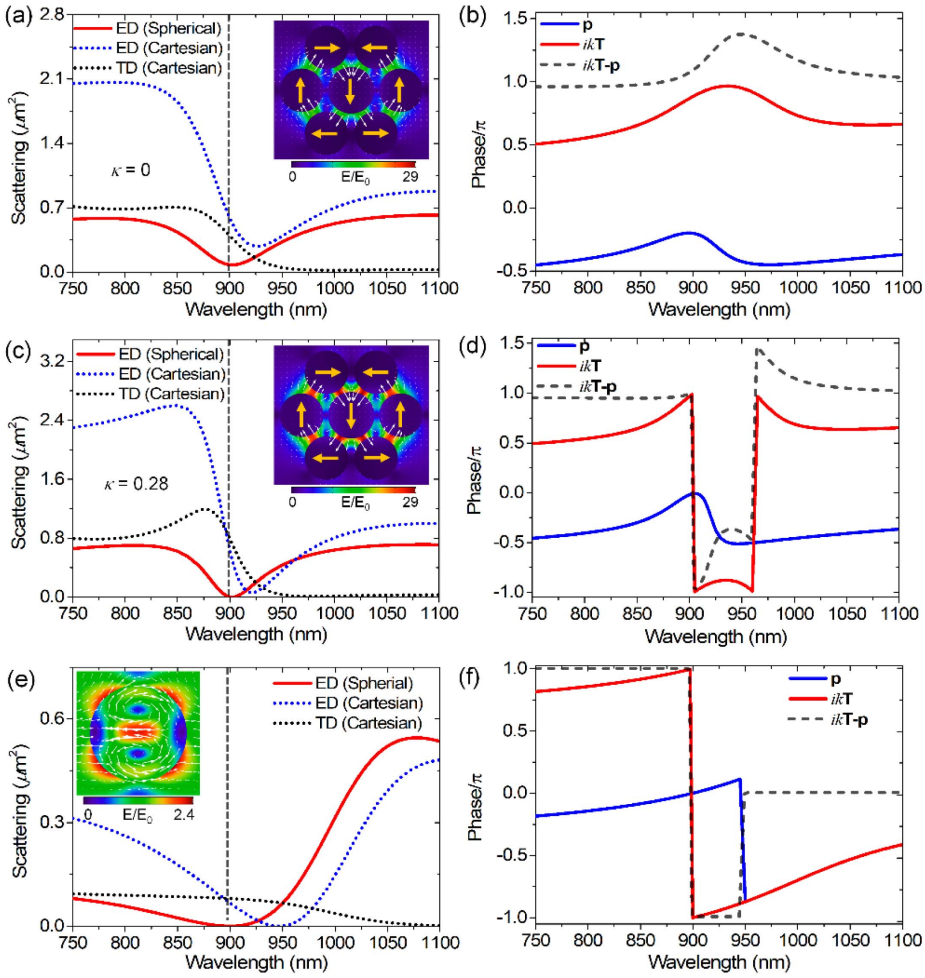

Fig. 2. Contributions of the spherical ED and the Cartesian ED and TD into the scattering cross sections of an Au–SiO_2 heptamer with the insets of near-field distributions E/E_0 on top of Au disks (at the plane of $z = 50$ nm) at 900 nm (a) for a passive nanosystem $\kappa = 0$ and (c) for an active nanosystem $\kappa = 0.28$. (e) Silicon nanosphere. The E-field directions and the polarized directions of Au metamolecules are indicated by the white arrows and the yellow arrows, respectively. (b), (d), and (f) Corresponding normalized phase of $\mathbf{p}$ and $ik\mathbf{T}$.

the high-refractive-index (silicon) nanoparticles. In addition, the excitation of anapole states in plasmonic systems can result in enhancement of the near fields in subwavelength spatial regions outside of nanoparticles. That is especially important for developments of nonlinear nanophotonic, plasmonic devices and functional metamaterials, which provide facilities for strong light energy concentration at the nanoscale. The tremendous near-field enhancements are advantageous for boosting Raman scattering [46], fluorescence [47], and nonlinear effects [15]. Moreover, compared to the high-refractive-index nanoparticles, the anapole mode can be excited in the metallic metamolecules with smaller volume.

4. COUPLED OSCILLATORS MODEL

In order to better understand the achievement of anapole condition via loss-compensation mechanism, we adopt an ECO model to analyze the process of the compensation of ohmic losses. In reality, the anapole mode belongs to the category of Fano resonance, which can be well characterized by the ECO model. Herein, the two-coupled oscillators model can be expressed as [38]

$$\ddot{x}_1 + \gamma_1\dot{x}_1 + \omega_1^2 x_1 - \upsilon_{12}x_2 = 0.5\ddot{P}_{\text{tot}} + \alpha_1 E_{\text{ext}}, \quad \textbf{(4)}$$

$$\ddot{x}_2 + \gamma_2\dot{x}_2 + \omega_2^2 x_2 - \upsilon_{21}x_1 = 0.5\ddot{P}_{\text{tot}} + \alpha_2 E_{\text{ext}}, \quad \textbf{(5)}$$

where x_1 and x_2 are the displacements from the equilibrium position of the first and second oscillators with the harmonic solution form of $x_1(t) = c_1 e^{i\omega t}$ and $x_2(t) = c_2 e^{i\omega t}$ [48]. γ_1 and γ_2 are the damping coefficients of the first and second oscillators accounting for intrinsic losses, respectively. ω_1 and ω_2 are the natural frequencies (eigenmodes) of the two oscillators. υ_{12} and υ_{21} describe the coupling strength between the two oscillators ($\upsilon_{12} = \upsilon_{21}$). $P_{\text{tot}} = \alpha_1 x(t) + \alpha_2 x(t)$ is the total dipole moment of the system describing the radiative damping, where α_1 and α_2 are the polarizabilities corresponding to the plasmon amplitude to their induced dipole moments. The oscillators are driven by the harmonic forces $\alpha_1 E_{\text{ext}}$ and $\alpha_2 E_{\text{ext}}$, where $E_{\text{ext}} = E_0 e^{i\omega t}$. Note that the first and second oscillators indicate the Cartesian ED and TD moments, respectively.

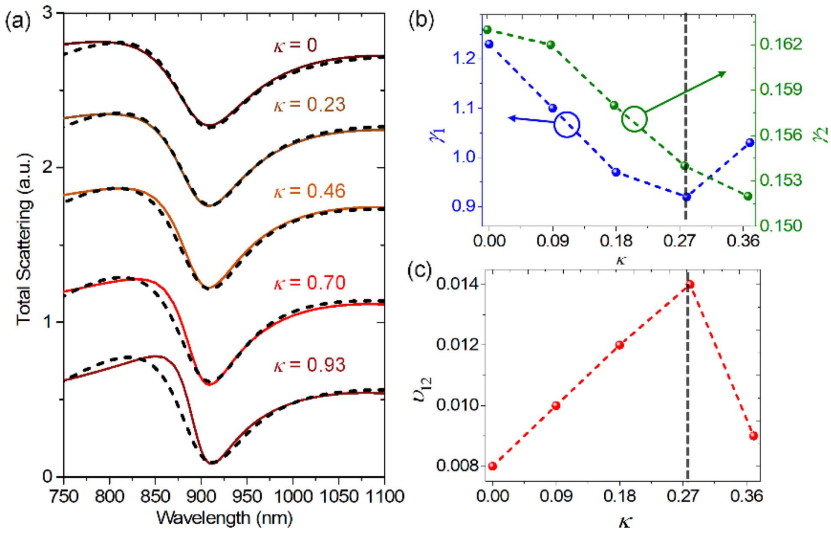

Fig. 3. (a) FEM calculation (solid curves) and ECO model fit (black dot curves) of the total scattering cross sections of an Au–SiO_2 heptamer with the gain coefficients varying from 0 to 0.37. (b) First oscillator (Cartesian ED moment) damping coefficient γ_1 and second oscillator (Cartesian TD moment) damping coefficient γ_2. (c) Coupling strength υ_{12}.

Table 1. Parameters from ECO Model for Different Gain Coefficients [Fig. 3(a)]

κ	E_0	α_1	α_2	γ_1	γ_2	ω_1	ω_2	υ_{12}
0	11.300	0.173	−0.008	1.230	0.163	1.675	1.387	0.008
0.09	10.800	0.170	−0.008	1.100	0.162	1.655	1.382	0.010
0.18	10.100	0.170	−0.008	0.970	0.158	1.630	1.380	0.012
0.28	10.100	0.168	−0.009	0.920	0.154	1.610	1.380	0.014
0.37	10.300	0.169	−0.009	1.030	0.152	1.630	1.385	0.009

The total scattering cross section is $|c_1 + c_2|^2$ [38], where c_1 and c_2 are obtained by solving Eqs. (4) and (5).

The total scattering spectra of the Au–SiO_2 heptamer are calculated via the FEM and ECO models, respectively. According to Fig. 3(a), the κ-dependent total scattering cross sections are well fitted by the ECO model (the fitting parameters from the ECO model are shown in Table 1). The first oscillator models the radiative mode, which has a high damping coefficient γ_1. In contrast, the second oscillator models the

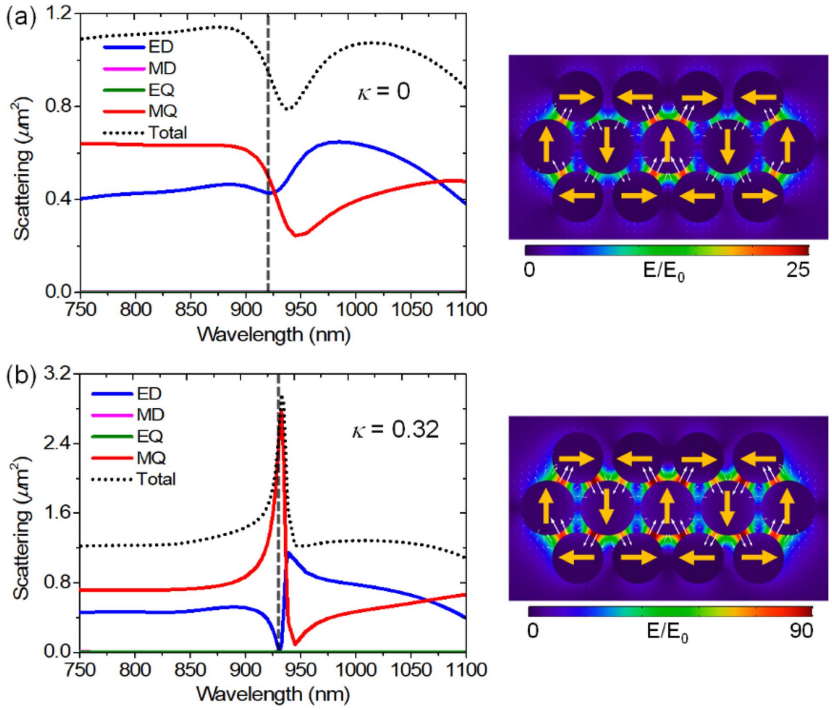

Fig. 4. Scattering cross sections and their spherical multipole decomposition calculated for Au-SiO_2 thirteen polymer with the near-field distribution E/E_0 on top of Au disks (at the plane of $z = 50$ nm) for an active nanosystem (a) $\kappa = 0$ and (b) $\kappa = 0.32$.

nonradiative mode with a low damping coefficient γ_2 ($\gamma_1 \gg \gamma_2$). The processes of loss compensation can be understood by the change trends of damping coefficients and the coupled strength of the oscillators. According to Fig. 3(b), the damping coefficients (γ_1 and γ_2) of the two oscillators decrease with the increase of gain coefficient. In other words, the compensation of ohmic losses leads to the decrease of total damping losses of the oscillators. Meanwhile, the decrease of the damping loss leads to the increase of the coupling strength between the two oscillators as shown in Fig. 3(c). However, when gain coefficient is higher than 0.28 ($\kappa > 0.28$), the damping loss of the first oscillator starts to increase. The damping loss of the second oscillator remains in decay. According to Fig. 3, the increase of damping loss of the first oscillator and the decrease of damping loss of the second one not only result in the stronger scattering peak of the low energy but also lead to the reduction of the coupling strength υ_{12}. Thus, when the gain coefficient reaches 0.28, the coupling strength between the two oscillators comes to its maximum value where the anapole condition is achieved, leading to the completely destructive interference.

5. HIGH-ORDER PLASMONIC ANAPOLE STATE

In addition, we also demonstrate that a high-order anapole state is also achieved in metallic metamolecules by increasing the coupling strength between Cartesian ED and TD moments. In Au–SiO_2 thirteen polymer, all the diameters of the center five disks are 208 nm, and the surrounding disks with the diameters of 195 nm are symmetrically distributed around the center disk with the separation $g = 20$ nm. Figures 4(a) and 4(b) indicate that if the gain coefficient reaches 0.32, the anapole state at about 931 nm is achieved. Besides, according to the near-field distributions of E/E_0 plotted in Figs. 4(a) and 4(b), the anapole state at 931 nm is the high-order anapole state. The enhancement of the induced near fields of high-order anapole mode origin is much stronger than that of low-order anapole mode origin, which suggests the superiority of the high-order mode in concentrating light in subwavelength regions. The excitation of the higher-order anapole state suggests that the anapole states supported by high-refractive-index particles [49] can be also achieved in the subtly designed metallic structures. Furthermore, the generation mechanisms of many nonlinear effects from different modes are vastly different, which makes great implications for the excitations of different anapole states. The excitations of low- and high-order anapole states greatly contribute to designing different types of functional metamaterials.

6. CONCLUSION

In summary, it has been theoretically shown that low- and high-order anapole states can be excited in metallic metamolecules. As both the electric and magnetic modes are supported by the metallic metamolecules, it offers the necessary conditions of the origin of the anapole states. The excitation of the ideal plasmonic anapole state depends on the effective excitation of the TD moment and fine-tuning it to ensure the completely destructive interference with the Cartesian ED moment. The totally destructive interference is achieved by enhancing the coupling strength. We have overcome a major limitation of plasmonic (metal) systems in realization of anapole states, related with strong ohmic absorption of light, by doping of the system by a gain material. Note that the spectral position and width of the gain effects depend on the materials used, and the environment and can vary widely. In this case, from the practical point of view, the implementation of the anapole state can be achieved in a required spectral gain range by adjusting the dimensions and material parameters of the total structure. The developed coupled oscillator model with active terms has been used for clarification of the physical process in the anapole state formation. Compared to the high-refractive-index nanoparticles, the plasmonic anapole modes can be excited in the metallic metamolecules with greater enhancement of near fields, which indicate the remarkable energy concentration performance and have more important implications for enhancing Raman scattering, fluorescence, and nonlinear effects. The theoretical results in this paper can be realized with the current nanofabrication technology, which not only open a route to study the anapole modes but also provide a new way of thinking to achieve the total suppression of noise modes and increase the signal-to-noise ratio of the target modes. Application of the considered structures, as buildings blocks for material developments, can extend varied physical approaches [50–52] to the creation of new materials and metamaterials with special functional properties.

Funding. Natural Science Foundation of Zhejiang Province (LQ21A040012); National Natural Science Foundation of China (11804323, 12004362); Deutsche Forschungsgemeinschaft (DFG, German Research Foundation) under Germany's Excellence Strategy within the Cluster of Excellence PhoenixD (390833453).

Acknowledgment. We thank Hai-Long Wang, Hai-Tao Liu, and Dong Xiang for their valuable suggestions.

Disclosures. The authors declare no conflicts of interest.

†These authors contributed equally to this work.

REFERENCES

1. T. J. Davis and D. E. Gomez, "Colloquium: an algebraic model of localized surface plasmons and their interactions," Rev. Mod. Phys. **89**, 011003 (2017).
2. G. Zengin, M. Wersäll, S. Nilsson, T. J. Antosiewicz, M. Käll, and T. Shegai, "Realizing strong light-matter interactions between single-nanoparticle plasmons and molecular excitons at ambient conditions," Phys. Rev. Lett. **114**, 157401 (2015).
3. A. B. Evlyukhin, C. Reinhardt, A. Seidel, B. S. Luk'yanchuk, and B. N. Chichkov, "Optical response features of Si-nanoparticle arrays," Phys. Rev. B **82**, 045404 (2010).
4. A. García-Etxarri, R. Gómez-Medina, L. S. Froufe-Pérez, C. López, L. Chantada, F. Scheffold, J. Aizpurua, M. Nieto-Vesperinas, and J. J. Sáenz, "Strong magnetic response of submicron silicon particles in the infrared," Opt. Express **19**, 4815–4826 (2011).
5. A. B. Evlyukhin, S. M. Novikov, U. Zywietz, R. L. Eriksen, C. Reinhardt, S. I. Bozhevolnyi, and B. N. Chichkov, "Demonstration of magnetic dipole resonances of dielectric nanospheres in the visible region," Nano Lett. **12**, 3749–3755 (2012).
6. A. Kuznetsov, A. Miroshnichenko, Y.-H. Fu, J. B. Zhang, and B. Luk'yanchuk, "Magnetic light," Sci. Rep. **2**, 492 (2012).

7. A. I. Kuznetsov, A. E. Miroshnichenko, M. L. Brongersma, Y. S. Kivshar, and B. Luk'yanchuk, "Optically resonant dielectric nanostructures," Science **354**, aag2472 (2016).
8. D. K. Gramotnev and S. I. Bozhevolnyi, "Plasmonics beyond the diffraction limit," Nat. Photonics **4**, 83–91 (2010).
9. N. J. Halas, S. Lal, W.-S. Chang, S. Link, and P. Nordlander, "Plasmons in strongly coupled metallic nanostructures," Chem. Rev. **111**, 3913–3916 (2011).
10. A. Krasnok, A. E. Miroshnichemko, P. A. Belov, and Y. Kivshar, "All-dielectric optical nanoantennas," Opt. Express **20**, 20599–20604 (2012).
11. A. E. Miroshnichenko, A. B. Evlyukhin, Y. F. Yu, R. M. Bakker, A. Chipouline, A. I. Kuznetsov, B. Luk'yanchuk, B. N. Chichkov, and Y. S. Kivshar, "Nonradiating anapole modes in dielectric nanoparticles," Nat. Commun. **6**, 8069 (2015).
12. T. Feng, Y. Xu, Z. Liang, and W. Zhang, "All-dielectric hollow nanodisk for tailoring magnetic dipole emission," Opt. Lett. **41**, 5011–5014 (2016).
13. A. K. Ospanova, I. V. Stenishchev, and A. A. Basharin, "Anapole mode sustaining silicon metamaterials in visible spectral range," Laser Photon. Rev. **12**, 1800005 (2018).
14. T. Feng, Y. Xu, W. Zhang, and A. E. Miroshnichenko, "Ideal magnetic dipole scattering," Phys. Rev. Lett. **118**, 173901 (2017).
15. G.-M. Pan, S. Ma, K. Chen, H. Zhang, L. Zhou, Z.-H. Hao, and Q.-Q. Wang, "Pure magnetic-quadrupole scattering and efficient second-harmonic generation from plasmon-dielectric hybrid nano-antennas," Nanotechnology **30**, 265202 (2019).
16. J. Tian, H. Luo, Y. Yang, F. Ding, Y. Qu, D. Zhao, M. Qiu, and S. I. Bozhevolnyi, "Active control of anapole states by structuring the phase-change alloy $Ge_2Sb_2Te_5$," Nat. Commun. **10**, 396 (2019).
17. C. M. Ho and R. J. Scherrer, "Anapole dark matter," Phys. Lett. B **722**, 341–346 (2013).
18. V. A. Fedotov, A. Rogacheva, V. Savinov, D. Tsai, and N. I. Zheludev, "Resonant transparency and non-trivial non-radiating excitations in toroidal metamaterials," Sci. Rep. **3**, 2967 (2013).
19. J. S. T. Gongora, A. E. Miroshnichenko, Y. S. Kivshar, and A. Fratalocchi, "Anapole nanolasers for mode-locking and ultrafast pulse generation," Nat. Commun. **8**, 15535 (2017).
20. Y. Yang and S. I. Bozhevolnyi, "Nonradiating anapole states in nanophotonics: from fundamentals to applications," Nanotechnology **30**, 204001 (2019).
21. K. V. Baryshnikova, D. A. Smirnova, B. S. Lukyanchuk, and Y. Kivshar, "Optical anapoles: concepts and applications," Adv. Opt. Mater. **7**, 1801350 (2019).
22. V. Savinov, N. Papasimakis, D. P. Tsai, and N. I. Zheludev, "Optical anapoles," Commun. Phys. **2**, 69 (2019).
23. I. E. Takou, A. C. Tasolamprou, O. Tsilipakos, Z. Viskadourakis, M. Kafesaki, G. Kenanakis, and E. N. Economou, "Anapole tolerance to dissipation losses in thermally tunable water-based metasurfaces," Phys. Rev. Appl. **15**, 014043 (2021).
24. R. Verre, D. G. Baranov, B. Munkhbat, J. Cuadra, M. Käll, and T. Shegai, "Transition metal dichalcogenide nanodisks as high-index dielectric Mie nanoresonators," Nat. Nanotechnol. **14**, 679–683 (2019).
25. S.-Q. Li and K. B. Crozier, "Origin of the anapole condition as revealed by a simple expansion beyond the toroidal multipole," Phys. Rev. B **97**, 245423 (2018).
26. E. A. Gurvitz, K. S. Ladutenko, P. A. Dergachev, A. B. Evlyukhin, A. Miroshnichenko, and A. S. Shalin, "The high-order toroidal moments and anapole states in all-dielectric photonics," Laser Photon. Rev. **13**, 1800266 (2019).
27. K. Marinov, A. D. Boardman, V. A. Fedotov, and N. Zheludev, "Toroidal metamaterial," New J. Phys. **9**, 324 (2007).
28. T. Kaelberer, V. A. Fedotov, N. Papasimakis, D. P. Tsai, and N. I. Zheludev, "Toroidal dipolar response in a metamaterial," Science **330**, 1510–1512 (2010).
29. A. B. Evlyukhin, T. Fischer, C. Reinhardt, and B. N. Chichkov, "Optical theorem and multipole scattering of light by arbitrarily shaped nanoparticles," Phys. Rev. B **94**, 205434 (2016).
30. L. Wei, Z. Xi, N. Bhattacharya, and H. P. Urbach, "Excitation of the radiationless anapole mode," Optica **3**, 799–802 (2016).
31. A. A. Basharin, M. Kafesaki, E. N. Economou, C. M. Soukoulis, V. A. Fedotov, V. Savinov, and N. I. Zheludev, "Dielectric metamaterials with toroidal dipolar response," Phys. Rev. X **5**, 011036 (2015).
32. A. C. Tasolamprou, O. Tsilipakos, A. Basharin, M. Kafesaki, C. M. Soukoulis, and E. N. Economou, "Chapter 7: Toroidal multipoles in metamaterials," in *Compendium on Electromagnetic Analysis from Electrostatics to Photonics: Fundamentals and Applications for Physicists and Engineers*, I. Tsukerman, ed. (World Scientific, 2019).
33. Z.-G. Dong, P. Ni, J. Zhu, X. Yin, and X. Zhang, "Toroidal dipole response in a multifold double-ring metamaterial," Opt. Express **20**, 13065–13070 (2012).
34. W. Liu, J. Zhang, and A. E. Miroshnichenko, "Toroidal dipole-induced transparency in core–shell nanoparticles," Laser Photon. Rev. **9**, 564–570 (2015).
35. W. Liu, J. Zhang, B. Lei, H. Hu, and A. E. Miroshnichenko, "Invisible nanowires with interfering electric and toroidal dipoles," Opt. Lett. **40**, 2293–2296 (2015).
36. F. Shafiei, F. Monticone, K. Q. Le, X.-X. Liu, T. Hartsfield, A. Alù, and X. A. Li, "A subwavelength plasmonic metamolecule exhibiting magnetic-based optical Fano resonance," Nat. Nanotechnol. **8**, 95–99 (2013).
37. G.-M. Pan, D.-J. Yang, L. Zhou, and Z.-H. Hao, "Low-loss resonance modes in a gain-assisted plasmonic multimer," J. Phys. D **51**, 115104 (2018).
38. A. Lovera, B. Gallinet, P. Nordlander, and O. J. F. Martin, "Mechanisms of Fano resonances in coupled plasmonic systems," ACS Nano **7**, 4527–4536 (2013).
39. R. Verre, Z. J. Yang, T. Shegai, and M. Käll, "Optical magnetism and plasmonic Fano resonances in metal-insulator-metal oligomers," Nano Lett. **15**, 1952–1958 (2015).
40. Z.-Y. Li and Y. Xia, "Metal nanoparticles with gain toward single-molecule detection by surface-enhanced Raman scattering," Nano Lett. **10**, 243–249 (2010).
41. M. A. Noginov, G. Zhu, A. M. Belgrave, R. Bakker, V. M. Shalaev, E. E. Narimanov, S. Stout, E. Herz, T. Suteewong, and U. Wiesner, "Demonstration of a spaser-based nanolaser," Nature **460**, 1110–1112 (2009).
42. P. B. Johnson and R. W. Christy, "Optical constants of the noble metals," Phys. Rev. B **6**, 4370–4379 (1972).
43. P. Grahn, A. Shevchenko, and M. Kaivola, "Electromagnetic multipole theory for optical nanomaterials," New J. Phys. **14**, 093033 (2012).
44. R. Alaee, C. Rockstuhl, and I. Fernandez-Corbaton, "An electromagnetic multipole expansion beyond the long-wavelength approximation," Opt. Commun. **407**, 17–21 (2018).
45. A. B. Evlyukhin and B. N. Chichkov, "Multipole decompositions for directional light scattering," Phys. Rev. B **100**, 125415 (2019).
46. R. Zhang, Y. Zhang, Z. C. Dong, S. Jiang, C. Zhang, L. G. Chen, L. Zhang, Y. Liao, J. Aizpurua, Y. Luo, J. L. Yang, and J. L. Yang, "Chemical mapping of a single molecule by plasmon-enhanced Raman scattering," Nature **498**, 82–86 (2013).
47. J. F. Li, C. Y. Li, and R. F. Aroca, "Plasmon-enhanced fluorescence spectroscopy," Chem. Soc. Rev. **46**, 3962–3979 (2017).
48. H. Chen, L. Shao, Y. C. Man, C. Zhao, J. Wang, and B. Yang, "Fano resonance in (gold core)-(dielectric shell) nanostructures without symmetry breaking," Small **8**, 1503–1509 (2012).
49. V. Zenin, A. Evlyukhin, S. Novikov, Y. Yang, R. Malureanu, A. Lavrinenko, B. Chichkov, and S. Bozhevolnyi, "Direct amplitude-phase near-field observation of higher-order anapole states," Nano Lett. **17**, 7152–7159 (2017).
50. E. Evlyukhin, E. Kim, D. Goldberger, P. Cifligu, S. Schyck, P. F. Weck, and M. Pravica, "High-pressure-assisted X-ray-induced damage as a new route for chemical and structural synthesis," Phys. Chem. Chem. Phys. **20**, 18949–18956 (2018).
51. Y. Sun, Z. Liu, P. Pianetta, and D.-I. Lee, "Formation of cesium peroxide and cesium superoxide on InP photocathode activated by cesium and oxygen," J. Appl. Phys. **102**, 074908 (2007).
52. E. Evlyukhin, E. Kim, P. Cifligu, D. Goldberger, S. Schyck, B. Harris, S. Torres, G. R. Rossman, and M. Pravica, "Synthesis of a novel strontium-based wide-bandgap semiconductor via X-ray photochemistry at extreme conditions," J. Mater. Chem. C **6**, 12473–12478 (2018).